Three-dimensional model for surface accumulation of chiral and nonchiral microswimmers

Danne M. van Roon, ^{1,2,*} Giorgio Volpe ⁰, ³ Margarida M. Telo da Gama ⁰, ^{1,2} and Nuno A. M. Araújo ⁰, ^{1,2,†} ¹Centro de Física Teórica e Computacional, Faculdade de Ciências, Universidade de Lisboa, 1749-016 Lisboa, Portugal ²Departamento de Física, Faculdade de Ciências, Universidade de Lisboa, 1749-016 Lisboa, Portugal ³Department of Chemistry, University College London, 20 Gordon Street, London WC1H 0AJ, United Kingdom

(Received 23 September 2024; accepted 11 March 2025; published 8 April 2025)

Persistent motion of microswimmers near boundaries is known to result in surface accumulation. A way to control surface accumulation is by reducing the contact surface area between swimmers and surface by modifying its topography, typically through the application of microscale structures. In this work, we introduce a three-dimensional (3D) phenomenological model of a microswimmer navigating a volume bounded by a top and bottom surface. We describe the swimmer-surface interaction with an effective near-surface alignment force, and study numerically the effect of surface textures, modeled by convex obstacles, on the surface accumulation of chiral and nonchiral microswimmers. We find that, depending on the angular velocity of the swimmer, and the alignment force, convex obstacles can either hinder or enhance surface accumulation. We discuss potential applications to sorting of microswimmers by their angular velocity.

DOI: 10.1103/PhysRevE.111.045405

I. INTRODUCTION

In the last two decades, active matter has become an increasingly important focus of research [1,2]. On small length scales, active matter describes micron-sized biological entities, such as bacteria, algi, and sperm cells, as well as artificial microswimmers including self-propelled Janus particles and active droplets [3]. Microswimmers are known to perform persistent directed motion when swimming in a volume (free from boundaries) [1,4,5]. When boundaries are present, they tend to accumulate at surfaces [3,6-9]. Steric effects and persistence in the swimming direction are known to be generic contributing factors leading to surface accumulation (or "trapping") in addition to hydrodynamic effects that depend on the specifics of the swimmer and the surface [10-12]. Driven by hydrodynamic interactions, various microswimmers have been observed to move in chiral trajectories typically along circles, when swimming near a flat interface. Examples include E. coli [13,14] and sperm cells [15] or artificial swimmers [10].

Bacterial surface dynamics are central in various industrial, biomedical, and environmental processes [16–18]. On the one hand, the adhesion of bacteria to surfaces frequently results in the formation of persistent biofilms that are difficult to remove, causing challenges in various fields, including fouling of water purification systems [19], corrosion of structures used to transport and store chemicals [20], and adhesion to medical implants, where bacterial infection can result in inflammation that can even lead to death [21]. On the other hand, the industrial potential of biofilms is becoming increasingly developed, including biorefineries [22], bioremediation

*Contact author: dvroon@fc.ul.pt †Contact author: nmaraujo@fc.ul.pt to remove contaminants from freshwater and wastewater [23], and as templates for new materials with applications in construction and industry [24].

A quantitative understanding of surface entrapment and subsequent adhesion could further the development of engineered materials to control and prevent bacterial adhesion to surfaces [25-28]. In recent years, the effects of surface topography and roughness on bacterial surface dynamics and adhesion have received increasing attention [6,8]. Experimental observations show that the topography of the environment can strongly influence the dynamics of microswimmers on a surface, in nonintuitive ways. Experimental evidence indicates that the presence of porous microstructures generally hinders the diffusive transport of microswimmers [29,30]. Interestingly, for chiral microswimmers, contrasting phenomenology has also been observed. For example, a significantly enhanced propagation on surfaces, due to randomly placed obstacles, has been reported in theoretical studies [31–33] and in experiments with $E.\ coli\ [5]$. Furthermore, experiments tracking E. coli navigating a colloidal crystal revealed that the colloids rectify the trajectories of the bacteria, resulting in enhanced transport [34–37].

Experiments on E. coli approaching a surface have shown that the average reorientation of the cells in a direction parallel to the surface is driven by steric forces at contact and short-ranged hydrodynamics, dominating any long-ranged hydrodynamics [6,38–40]. Similar results were obtained for sperm cells on a surface [41], for E. coli interacting with micron-sized pillars [12], and for synthetic microswimmers navigating an environment of passive colloidal beads [10]. After the reorientation event, a swimmer was observed to move along a boundary (surface, pillar, or bead) until Brownian diffusion rotates its axis away.

From a numerical perspective, detailed simulations of the swimmer dynamics, which explicitly include the coupling between the swimmer and surrounding fluid along with hydrodynamic effects, are extremely demanding. Instead, to reach the relevant timescales of the dynamics, effective models are used, where the details of the interactions are coarse grained into mechanistic descriptions [3,5,30–33,42–45]. Many numerical models consider 2D systems, but some have also considered 3D [46]. For example, in [47], the authors introduced a 3D model describing the behavior of chemical microswimmers designed to model chemically active colloids. In [37] a bacterial cell was modeled in 3D by simulating the Brownian dynamics of a stiff polymer described as a bead-spring model.

In this article, we introduce a phenomenological 3D model to investigate the surface accumulation of microswimmers. The model accounts for the self-propagation of a swimmer and its tendency to swim in chiral (circular) trajectories when moving close to a surface. Approximating the motion of rodlike cells, the swimmer's motion is limited to moving along its direction of self-propagation. To represent the reorientation along boundaries, an effective short-ranged hydrodynamic force is introduced that aligns the propagation direction with the nearest boundary. E. coli and bull sperm cells are used as example microswimmers, navigating a volume bounded by a top surface plane and a bottom one, akin to a microfluidic channel. We study the effect of placing convex obstacles, which are three times the size of the swimmers, randomly on both surfaces, and examine how the surface accumulation is impacted by the strength of the alignment force and the angular velocity of the motion. The surface accumulation is quantified by measuring the fraction of swimmers near the surfaces. Our results show that the presence of obstacles always reduces the accumulation of nonchiral microswimmers on these surfaces, as, by aligning along the boundary of the obstacles, the swimmers are directed away from the surface. As the obstacle density is increased, the surface accumulation is reduced. For chiral microswimmers, the accumulation can be reduced or enhanced. As previously observed in [10–12], our model confirms that a chiral swimmer may get trapped orbiting an obstacle. This orbital trapping results from the interplay between the angular velocity and the alignment force along the boundary of the obstacle, and occurs only if the obstacles are at least equal to the size of the swimming orbit. We discuss how obstacles can be used to control the accumulation of chiral swimmers near surfaces by carefully tuning their size and, in addition, how obstacles can be employed to sort swimmers based on their angular velocity.

II. MODEL

We consider a spherical microswimmer of diameter σ (typically 1–5 µm for natural and synthetic microswimmers) moving with velocity \vec{v} and corresponding momentum \vec{p} . The swimmer navigates a volume of thickness 100σ bounded by a top and bottom square surface plane with edge size L and periodic boundary conditions along the directions parallel to the surfaces. Each surface plane is covered with $N_o = 100$ nonoverlapping obstacles of diameter $\sigma_o = 6\sigma$, uniformly and randomly placed on the surface so that their centers are on the surface plane. The obstacles are quantified by their surface coverage defined as $\rho = \frac{N_o \pi \sigma_o^2}{4T^2} (\times 100\%)$. Motion of the

swimmer is determined by the deterministic force acting on it and by a stochastic term $\vec{\xi}$ representing fluctuations in the direction of motion.

The phenomenological model separately accounts for three distinct observations of microswimmers near surfaces: the swimmer's self-propagation or "activity," alignment of the direction of self-propagation along boundaries, and the tendency to move in circular trajectories when close to a surface. The motion of a swimmer, resulting from self-propagation and viscous drag is determined by

$$\vec{F}_{\text{active}} = -\frac{1}{\tau} (\vec{p} - p_0 \hat{p}), \tag{1}$$

which describes its tendency to move with a momentum of magnitude p_0 along the direction of \vec{p} , given by the unit vector $\hat{p} = \frac{\vec{p}}{|\vec{p}|}$. Corrections to possible deviations from the self-propagation occur in a timescale set by τ . Notice that, for $t > \tau$, the dynamics of the microswimmer is overdamped.

The tendency to align with the substrate is described by

$$\vec{F}_{\text{alignment}} = -\alpha(\hat{p} \cdot \hat{\mu}_{\perp})\hat{\mu}_{\perp},\tag{2}$$

representing an effective reorientation observed for microswimmers approaching a boundary. The strength of the alignment is determined by α . For $\alpha>0$, the force will tend to align the swimmer along the obstacle boundary or surface plane, with $\hat{\mu}_{\perp}$ the unit vector perpendicular to the obstacle boundary or surface plane closest to the swimmer.

The tendency to perform a chiral motion near a surface is described by

$$\vec{F}_{\text{chiral}} = \beta(\hat{p} \times \hat{\mu}_{\perp}), \tag{3}$$

where β sets the angular velocity. For $\beta > 0$, the swimmer will follow circular trajectories when moving close to the surface. The orbital radius of the trajectories R_{orbit} is determined by β and defined as $R_{\text{orbit}} = \frac{v}{\beta}$. We introduce $\Omega = \frac{\sigma_0}{2R_{\text{orbit}}}$ as a measure of the angular velocity, by normalizing the size of the obstacles with the size of the swimming orbit. For larger values of β , swimmers trace smaller orbits corresponding to larger values of Ω . A schematic illustration of a nonchiral swimmer ($\beta = 0$) is shown in Fig. 1(a)(I), and an illustration of a chiral swimmer in Fig. 1(b)(I). To represent the short-ranged nature of the interactions with boundaries, a cut-off distance $r_c = \frac{3\sigma}{2}$ is introduced so that, when the distance r between swimmer and the obstacle boundary or surface plane is $r > r_c$, α and β are set to 0.

The steric interaction has two components. A truncated Weeks-Chandler-Anderson potential is used to represent the steric interaction with the obstacles $\vec{F}_{\text{obstacle}} = -\nabla V$,

$$V(r_i) = \begin{cases} 4\left[\left(\frac{\sigma}{r_i}\right)^6 - \left(\frac{\sigma}{r_i}\right)^{12}\right] + 1 & \text{for: } r_i < 2^{\frac{1}{6}}\sigma, \\ 0 & \text{for: } r_i \geqslant 2^{\frac{1}{6}}\sigma, \end{cases}$$
(4)

where r_i is the distance between the swimmer and obstacle i. The WCA potential is a well tried method for including obstacle-swimmer interactions [5,33]. For the surface we use an exponential repulsion of magnitude

$$\vec{F}_{\text{surface}} = \frac{1}{r_{\text{s}}} \exp\left(-r_{\text{s}}\right),\tag{5}$$

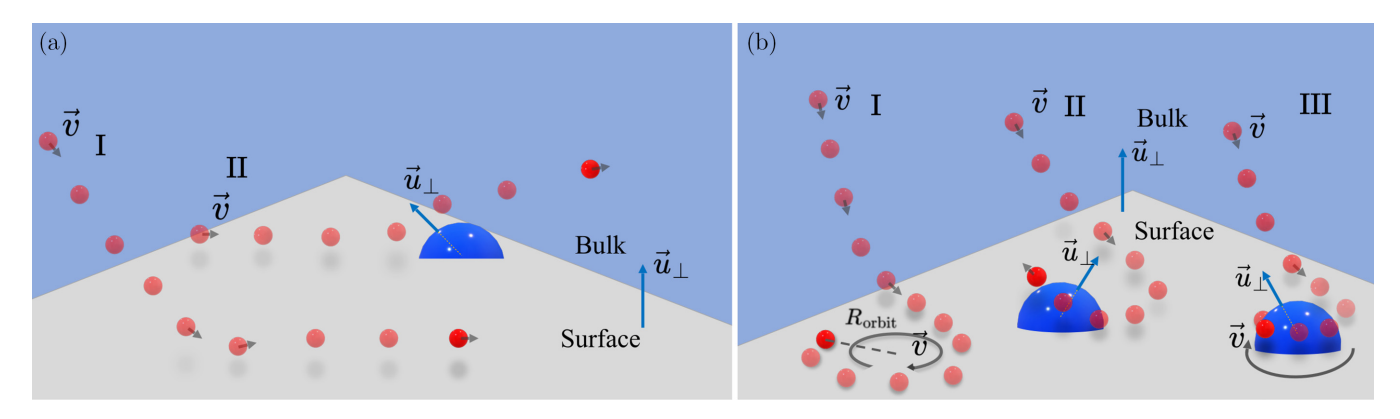


FIG. 1. [(a),(b)] Schematic depiction of a swimmer (red dots) moving at velocity \vec{v} in the volume (blue) near the surface (light gray): (a) a nonchiral swimmer (I) approaching the surface, and (II) guided away from the surface after interacting with an obstacle (dark blue hemisphere); (b) a chiral swimmer ($\Omega \neq 0$) (I) approaching the surface, where it moves in orbits of radius R_{orbit} , (II) guided away from the surface after interacting with the obstacle, and (III) trapped in an orbit around the boundary of the obstacle. The dark gray arrows indicate the direction of motion of the swimmer, while the blue arrows indicate the vector perpendicular to the closest surface plane or the boundary of the closest obstacle.

with r_s the distance between swimmer and surface. The interaction becomes effective when $r_s < \frac{\sigma}{2}$.

If we group terms that result from the swimmer-boundary interaction under $\vec{F}_{boundary}$,

$$\vec{F}_{\text{boundary}} = -\alpha(\hat{p} \cdot \hat{\mu}_{\perp})\hat{\mu}_{\perp} + \beta(\hat{p} \times \hat{\mu}_{\perp}) + \vec{F}_{\text{steric}}, \quad (6)$$

the trajectory of the swimmer can be obtained by integrating the following equation:

$$\dot{\vec{p}} = \vec{F}_{\text{active}} + \vec{F}_{\text{boundary}} + \vec{\xi}. \tag{7}$$

The fluctuations in the direction of motion $\vec{\xi}$ are implemented by rotating the swimmer perpendicular to its direction of self-propagation \hat{p} . There is no translational diffusion ($D_{\rm T}=0$). A rotation is generated by assigning to \hat{p} a new direction uniformly and randomly drawn from the spherical cap centered around \hat{p} with unit radius. The amplitude of the fluctuations can be tuned by changing the (polar) angle of the cap to obtain the proper rotational diffusion constant. The effective diffusion constant $D_{\rm R}$ is extracted through a linear regression of the mean squared displacement (MSD) at long times

$$MSD(t) \sim 6D_R t$$
. (8)

In our case, we performed the linear regression in the interval $3000\tau < t < 3600\tau$.

The time evolution of the system is obtained by integrating its equation of motion with the velocity Verlet method. In the following we will express distances in terms of the dimensionless swimmer radius $\sigma/2$ and time in terms of τ which sets the characteristic time of the motile force [Eq. (1)]. Finally, the step size in the simulation is $\Delta t = 10^{-4}$, and a simulation lasts for $t = 3600 \, \tau$.

III. RESULTS

At the beginning of the simulation, swimmers are positioned randomly and uniformly within the simulation volume. During the simulation, depending on the parameters, the swimmers will accumulate at the surfaces (or not) which will determine the steady state distribution. To characterize the surface accumulation, we count the number of microswimmers

 $N_{\rm surface}$ that are at a distance shorter than 3σ (one obstacle radius) from the bottom or top surfaces in the steady state of the system. We define the fraction ϕ of microswimmers accumulated at the surfaces as

$$\phi = \left(\frac{N_{\text{surface}}}{N}\right). \tag{9}$$

The brackets $\langle . \rangle$ indicate an ensemble average over N swimmers (the swimmers do not interact). For smooth surfaces $(\rho=0)$, the surface planes contain no obstacles and results given for this case are obtained from averaging $N=25\,000$ swimmers. For surfaces with obstacles, results are obtained by averaging over the same number of swimmers for each value of obstacle density. In particular, we simulate 100 different obstacle configurations with 250 swimmers per configuration. We consider two different values of the rotational diffusion coefficient: $D_R=0.1\,\mathrm{rad}^2/\mathrm{s}$ (Péclet number Pe = 120) corresponding to the rotational diffusion measured for $E.\ coli\ [40]$, and $D_R=10^{-4}\,\mathrm{rad}^2/\mathrm{s}$ (Pe = 1.2 10^5) corresponding to the value for bull sperm cells [41].

A. Smooth surface

To set the stage we first consider the simplest case of nonchiral ($\Omega=0$) swimmers navigating a volume bounded by smooth surfaces, where the surface accumulation ϕ increases with the dimensionless alignment force strength $\tau\alpha$. Figures 2(a) and 2(b) (blue diamonds) show how the surface accumulation ϕ increases with $\tau\alpha$ ranging from $\tau\alpha=0$, where the rotational diffusion governs the dynamics, to $\tau\alpha=60$, where the alignment force dominates. This range of $\tau\alpha$ covers the phenomenology of the model, for $\tau\alpha>60$ no new phenomenology was observed.

In the absence of alignment force ($\tau \alpha = 0$), about 15% $[D_R = 10^{-4} \text{ rad}^2/\text{s}$, Fig. 2(a)] and 12% $[D_R = 0.1 \text{ rad}^2/\text{s}$ Fig. 2(b)] of the swimmers accumulate near the surface. This accumulation is a result of their persistent motion. A swimmer explores the volume until it collides with one of the surfaces, where it will stay until rotational diffusion directs it away from it so that it can escape.

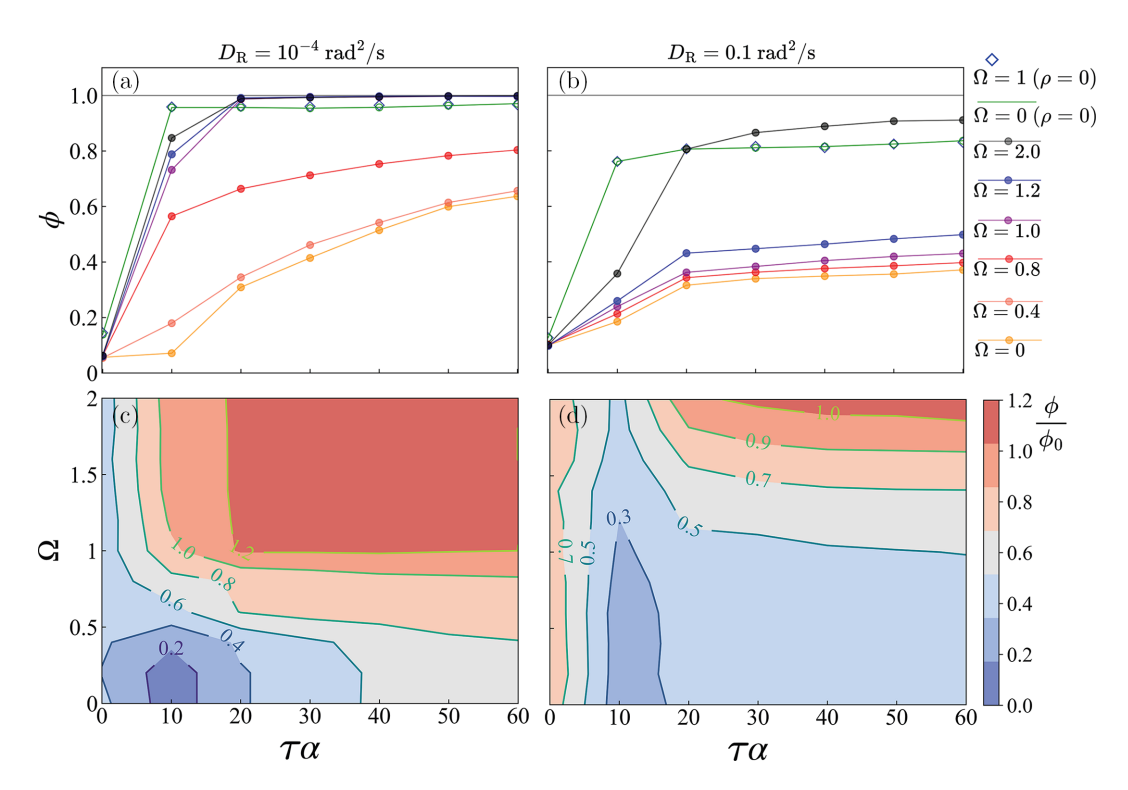


FIG. 2. [(a),(b)] Fraction of swimmers accumulated on the surface ϕ against the alignment force $\tau\alpha$ for different angular velocities Ω with an obstacle surface coverage $\rho=20\%$: (a) for swimmers with $D_R=10^{-4}$ rad²/s and (b) for swimmers with $D_R=0.1$ rad²/s. The colored lines denote the different angular velocities of the microswimmers on such surfaces. The green lines $(\Omega=0)$ and blue diamonds $(\Omega=1)$ denote surfaces without obstacles $(\rho=0)$ instead. [(c),(d)] Fraction $\frac{\phi}{\phi_0}$ of swimmers accumulated on a surface with convex obstacles relative to the fraction accumulated at a smooth surface ϕ_0 , as a function of Ω and $\tau\alpha$, (c) for $D_R=10^{-4}$ rad²/s and (d) for $D_R=0.1$ rad²/s. For weak alignment forces, the obstacles reduce the surface accumulation. The swimmer aligns with the obstacle boundary and is directed away from the surface. With increasing alignment forces, the surface accumulation increases. As the tendency of the swimmer to align along a surface is increased, detachments (due to Brownian diffusion) become rarer resulting in an increased accumulation. With increasing angular velocity, the surface exploration decreases, limiting the effect of the obstacles. The difference between the green line (surface without obstacles) and the other curves is reduced in (a) and (b). For sufficiently large alignment force and angular velocity, swimmers tend to align along the boundary of an obstacle and become trapped in orbits along its boundary, resulting in obstacles enhancing the surface accumulation. For $D_R=10^{-4}$ rad²/s in (a), this occurs for $\tau\alpha \geqslant 20$, where the curves $\Omega \geqslant 1$ cross above the green line and in (c) where $\frac{\phi}{\phi_0} > 1$. For $D_R=0.1$ rad²/s in (b) obstacles enhance the accumulation for $\tau\alpha \geqslant 20$, when the curve $\Omega \geqslant 2$ crosses above the green line and in (d) when $\frac{\phi}{\phi_0} > 1$.

As the alignment force increases, the fraction of swimmers accumulated near the surfaces increases. This behavior can be explained by considering that the alignment force competes with the rotational diffusion, as a stronger tendency to align prevents the swimmer from orienting away from the surface and escape. The marked increase in accumulation for $0 < \tau \alpha < 10$ results from a shift in the balance of this competition. For $D_R = 10^{-4}$ rad²/s [Fig. 2(a)] when $\tau \alpha \ge 10$, the alignment force becomes strong enough to trap the swimmer at the surface. The trapping results in an enhanced accumulation, which increases with the alignment force, reaching 95% for $\tau \alpha \ge 10$. When $D_R = 0.1$ rad²/s [Fig. 2(b)], the tendency of the swimmers to diffuse away from the surface is stronger, reducing the accumulation. The accumulation reaches 76% for $\tau \alpha = 10$ continuing to increase slowly to 82% for $\tau \alpha = 60$.

When chiral swimmers are considered ($\Omega \neq 0$), the accumulation behavior is unchanged for smooth surfaces. We consider various values of angular velocity between $\Omega=0.4$ (corresponding to a swimming orbit $R_{\rm orbit}=7.5\sigma$) and $\Omega=2$ ($R_{\rm orbit}=1.5\sigma$) which are consistent with values in the literature [13–15]. For much larger Ω , when $R_{\rm orbit}<\sigma$, a swimmer

effectively rotates around its axis, our model is no longer expected to capture the dynamics. In Figs. 2(a) and 2(b), the green line shows the accumulation for $\Omega=1$, which coincides with the blue diamonds for nonchiral swimmers ($\Omega=0$). The chirality causes the swimmers to trace circular trajectories along the surface, but does not affect their overall surface accumulation.

B. Surface structured with convex obstacles

A very different behavior is observed, for both values of $D_{\rm R}$, when randomly placed obstacles are added to the surface. We begin by considering swimmers with $D_{\rm R} = 10^{-4} \, {\rm rad}^2/{\rm s}$.

For nonchiral and chiral swimmers in a volume bounded by surfaces with obstacle density $\rho=20\%$, the accumulation near the surfaces [lines with circles in Fig. 2(a)] is reduced for all $\tau\alpha$ for $\Omega<1$, and for $\tau\alpha\leqslant 10$ for $\Omega\geqslant 1$. Figure 2(c) shows the fraction $\frac{\phi}{\phi_0}$ of swimmers that accumulate near a surface with obstacles (ϕ) with respect to a smooth surface (ϕ_0) as a function of the alignment force $\tau\alpha$ and angular velocity Ω .

For nonchiral swimmers and chiral swimmers with $0 \le$ $\Omega \leqslant 1$, the reduction of the surface accumulation by the obstacles $\left[\frac{\phi}{\phi_0} < 1\right]$ in Fig. 2(c)] is a result of the modified surface structure. In the absence of an alignment force ($\tau \alpha = 0$), about 8% of the swimmers accumulate at the surface. This accumulation is a result of their persistent motion, and the decrease in accumulation relative to the smooth surface can be attributed to the reduction of the flat surface area available to the swimmers because of the presence of the obstacles. For $\tau \alpha > 0$, when approaching an obstacle, a swimmer aligns its direction of motion along its convex boundary instead of the surface plane, so that its orientation is directed away from the surface. As $\tau \alpha$ is increased, the tendency to align along the surface or boundary of an obstacle becomes stronger, increasing the surface accumulation. A schematic trajectory that leaves the surface after aligning along an obstacle is shown for a nonchiral swimmer in Fig. 1(a)(II) and a chiral swimmer in Fig. 1(b)(II). For $0 \le \Omega < 1$, the accumulation increases with the angular velocity [Fig. 2(a). This can be explained by the chiral swimmers exploring the surface less extensively, thereby encountering fewer obstacles when compared to less chiral swimmers. As the angular velocity increases, the swimming orbits become smaller, decreasing the efficiency with which the surface is explored. This limits the ability of the obstacles to reduce the accumulation at the surface and leads to an increase of $\frac{\phi}{\phi_0}$ with the angular velocity in Fig. 2(c).

For chiral swimmers with a larger angular velocity ($\Omega \geqslant 1$) a different behavior is observed, where swimmers move in persistent orbits along the boundary of an obstacle, until the rotational diffusion directs them away from it and they can escape. A schematic example trajectory of a swimmer that orbits an obstacle is displayed in Fig. 1(b)(III). For $D_R = 10^{-4} \text{ rad}^2/\text{s}$, the rotational diffusion is relatively weak and the swimmers can become effectively trapped at the obstacles for a sufficiently strong alignment force $\tau \alpha \geqslant 20$, increasing the surface accumulation in Fig. 2(a). We note that due to this "orbital trapping," the ability of the obstacles to direct swimmers away from the surface is mitigated for $\tau \alpha \geqslant 20$, whereby obstacles will rather enhance surface accumulation $[\frac{\phi}{\phi_0} > 1 \text{ in Fig. 2(c)}].$

The trapping of a swimmer in an orbit around an obstacle is a result of the interplay between the angular velocity and the alignment force. When a swimmer approaches an obstacle, the alignment force will guide the swimmer around its boundary. For a swimming orbit that is of the size or smaller than the size of the obstacle ($\Omega \ge 1.0$), the angular velocity will continuously direct the swimmer toward its center with the alignment force directing the swimmer back along the boundary. A larger angular velocity will result in a stronger tendency to align along the boundary, enhancing the entrapment effect. Detachment of a swimmer from an orbit can occur when the Brownian diffusion is effective in reorienting the swimmer to escape from its orbit.

For $D_R = 0.1 \text{ rad}^2/\text{s}$, the larger rotational diffusion randomizes the motion, increasing the boundary detachment and reducing surface accumulation [Fig. 2(b)]. By perturbing the circular trajectories, the diffusion increases the surface exploration of chiral swimmers, reducing the difference between different angular velocities Ω . Due to enhanced surface

exploration, obstacles become more effective in reducing near surface accumulation of chiral swimmers, decreasing $\frac{\phi}{\phi_0}$ in Fig. 2(d) [when compared to $D_{\rm R}=10^{-4}~{\rm rad}^2/{\rm s}$ in Fig. 2(c)] for all but $\tau\alpha<10$ when the alignment force is weak and diffusion dominates.

The effect of orbital trapping on surface accumulation is reduced significantly for most values of Ω . The diffusion breaks the orbits reducing the surface accumulation promoted by the obstacles $\left[\frac{\phi}{\phi_0} < 1\right]$ in Fig. 2(d)] with the exception of $\Omega = 2$, where the angular velocity is strong enough to keep the swimmer aligned along the boundary of an obstacle, effectively trapping it for $\tau \alpha > 20$ [$\frac{\phi}{\phi_0} > 1$ in Fig. 2(d)].

C. Effect of the obstacle density on accumulation

Now we proceed to examine the effect of the obstacle density ρ . In Figs. 3(a) and 3(b) $\frac{\phi}{\phi_0}$, the fraction of accumulated swimmers is presented for alignment force strengths $\tau\alpha=10$ (triangles) and $\tau\alpha=60$ (circles).

An increase in the density enhances the effect of the obstacles on the surface accumulation. The accumulation declines with increasing density for $\tau\alpha$ and Ω where obstacles repel swimmers from the surface $[\frac{\phi}{\phi_0} < 1$ in Figs. 2(c) and 2(d)] and increases where orbital trapping dominates the dynamics $[\frac{\phi}{\phi_0} > 1$ in Figs. 2(c) and 2(d)].

As the angular velocity Ω increases, $\frac{\phi}{\phi_0}$ varies more weakly with the density in Figs. 3(a) and 3(b). For swimmers with small angular velocities, the accumulation declines rapidly for small densities before continuing to slowly decline. Due to the more efficient space exploration of swimmers with a small angular velocity, a lower density of obstacles is sufficient to affect the accumulation. This suggest that obstacles are effective in detaching swimmers with small angular velocities from the surface even at low densities. For swimmers with larger angular velocity, space exploration is less efficient, as increasing the density gradually increases the effect of the obstacles, and larger densities are required to affect the surface accumulation.

When we compare $D_R = 10^{-4} \, \mathrm{rad}^2/\mathrm{s}$ [Fig. 3(a)] and $D_R = 0.1 \, \mathrm{rad}^2/\mathrm{s}$ [Fig. 3(b)], we note that for $D_R = 0.1 \, \mathrm{rad}^2/\mathrm{s}$ increasing the obstacle density has a larger effect on $\frac{\phi}{\phi_0}$ for most values of the angular velocity Ω , suggesting that the density dominates the accumulation behavior.

D. Sorting swimmers by angular velocity

By controlling the accumulation of microswimmers, obstacles may be used to sort swimmers of different angular velocity [42,48–50]. Depending on the angular velocities, the swimmers will tend to accumulate near a surface or remain in the volume with a different probability. For simplicity we will assume that the swimmers in the mixture are identical in all aspects but their angular velocity, and study the efficiency of the separation as a function of the alignment force and the different angular velocities of the mixture.

A way to sort swimmers of different angular velocities would be to consider obstacle sizes such that $\Omega < 1$ for one fraction (A) of swimmers and $\Omega > 1$ for the other (B). We define $\delta = \Omega_A - \Omega_B$ the resolution of the sorter and $\frac{\phi_A}{\phi_B}$ its

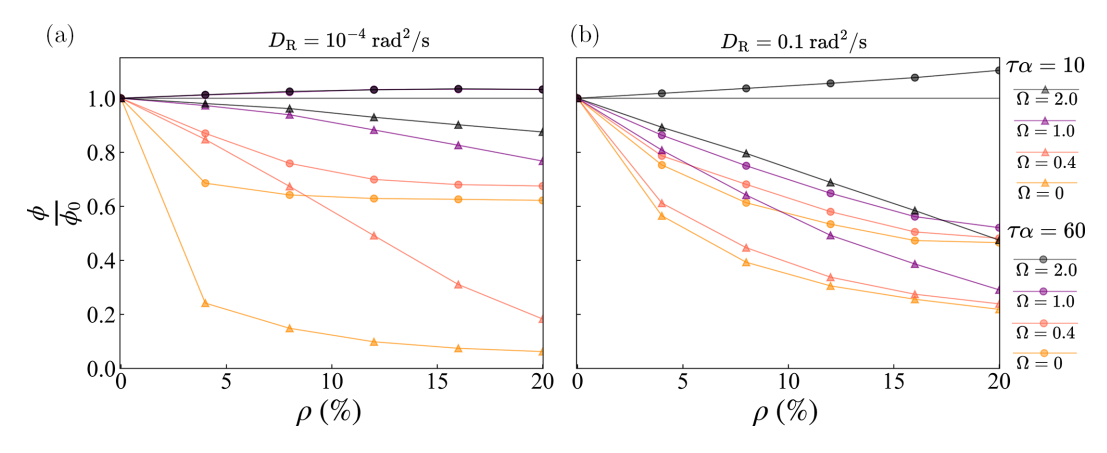


FIG. 3. Fraction ϕ of swimmers accumulated near the surface for a given angular velocity Ω normalized to ϕ_0 , the accumulation near a smooth surface for the same angular velocity, against the obstacles density ρ . The rotational diffusion is (a) $D_R = 10^{-4} \text{ rad}^2/\text{s}$ and (b) $D_R = 0.1 \text{ rad}^2/\text{s}$ with alignment force strengths $\tau \alpha = 10$ (triangles) and $\tau \alpha = 60$ (circles). As the density is increased the effect of the obstacles increases. For most cases the obstacles decrease the surface accumulation ($\frac{\phi}{\phi_0} < 1$). For $D_R = 10^{-4} \text{ rad}^2/\text{s}$, $\tau \alpha = 60$, and $\Omega \geqslant 1$, swimmers get trapped in orbits along the boundary of an obstacle, resulting in obstacles enhancing the accumulation ($\frac{\phi}{\phi_0} > 1$). For $D_R = 0.1 \text{ rad}^2/\text{s}$ this occurs at $\tau \alpha = 60$ and $\Omega = 2$.

efficiency, where Ω_A (Ω_B) and ϕ_A (ϕ_B) are, respectively, the angular velocity and surface accumulation fraction of swimmers A (B). In Figs. 4(a) and 4(b) the efficiency is displayed for swimmers with $D_R = 10^{-4} \text{ rad}^2/\text{s}$ and $D_R = 0.1 \text{ rad}^2/\text{s}$ for different values of the resolution δ and the alignment force strength $\tau \alpha$.

We observe that, as the rotational diffusion increases, the ability to sort the swimmers by angular velocity is reduced. For $D_{\rm R}=10^{-4}~{\rm rad^2/s}$ [Fig. 4(a)] the more chiral fraction accumulates up to 11 times as much as the less chiral one, whereas for $D_{\rm R}=0.1~{\rm rad^2/s}$ [Fig. 4(b)] the more chiral fraction accumulates by up to 2.5 times than the less chiral one.

For $D_{\rm R}=10^{-4}~{\rm rad}^2/{\rm s}$ and $\tau\alpha\approx 10$ the fraction with a higher angular velocity accumulates significantly more than the other fraction and the mixture can be sorted, while, for other $\tau\alpha$ values, the sorter becomes less efficient as $\tau\alpha$ increases. For $D_{\rm R}=0.1~{\rm rad}^2/{\rm s}$ the alignment force strength needs to be above 20 for the two fractions to

accumulate at different rates, and the sorter does not work efficiently.

IV. CONCLUSION

We have introduced a 3D model to study the surface accumulation of microswimmers, induced by steric forces and an effective short-ranged hydrodynamic force that aligns the propagation direction of the swimmer along the nearest boundary (surface or obstacle). Chiral and nonchiral microswimmers were considered, navigating a volume bounded by a bottom and a top surface plane. We introduced obstacles on the surfaces and studied their effect on the surface accumulation

For smooth surfaces (without obstacles) and structured surfaces (with obstacles), the surface accumulation is enhanced by increasing the alignment force. The alignment force competes with diffusion to prevent the swimmer (chiral and

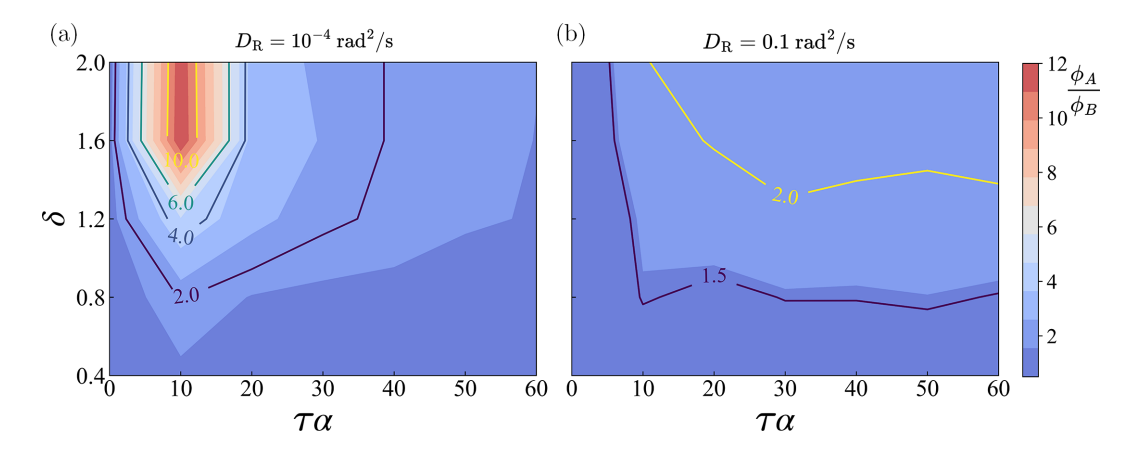


FIG. 4. Sorting efficiency $\frac{\phi_A}{\phi_B}$ of a mixture consisting of swimmers with angular velocities Ω_A and Ω_B with accumulations ϕ_A and ϕ_B for two values of the rotational diffusion: (a) $D_R = 10^{-4} \text{ rad}^2/\text{s}$ and (b) $D_R = 0.1 \text{ rad}^2/\text{s}$. The sorting efficiency is displayed as a function of the alignment force $\tau \alpha$, and the resolution of the sorter $\delta = \Omega_A - \Omega_B$. For $D_R = 10^{-4} \text{ rad}^2/\text{s}$ the sorter achieves an efficiency of ten, indicating that the fraction with the higher angular velocity accumulates ten times as much as the fraction with the lower angular velocity. For $D_R = 10^{-4} \text{ rad}^2/\text{s}$ the sorter is much less effective, reaching a maximum efficiency of two.

nonchiral) from orienting away from the surface and escaping. When obstacles are added to the surface, the angular velocity of the swimmer is found to strongly affect their accumulation. For a nonchiral swimmer, the obstacles significantly reduce the accumulation when compared to a smooth surface, even when a small fraction of the surface is covered by obstacles. The obstacles prevent a swimmer from aligning with the surface, by guiding it away into the volume, consistent with recent experimental results [5]. For a chiral swimmer, the ability of obstacles to mitigate the accumulation is reduced with increasing angular velocity. Swimmers with a large angular velocity explore the surface less efficiently, encountering fewer obstacles, which reduces their effect. Moreover, for a chiral swimmer we find that for sufficiently strong alignment forces, the swimmer may be trapped in a trajectory along the boundary of the obstacle [11,12,51], resulting in enhanced accumulation. We find that the relevant length scale for trapping is set by the obstacle size, so that, when the swimming orbit is of the size of the obstacle or smaller, trapping can occur. We further note that, for swimmers that experience a stronger rotational diffusion, the motion becomes more randomized, reducing the effect of the angular velocity on the accumulation.

The ability of obstacles to impact the accumulation of microswimmers at a surface may be used to guide the development of materials that selectively hinder or promote the adhesion of microswimmers, e.g., to control the establishment of biofilms in the case of bacteria. Our findings indicate that, by adding obstacles for nonchiral swimmers, a surface can become more resistant to accumulation, which is in line with studies of bacterial accumulation [6]. For chiral swimmers, the way obstacles impact surface accumulation of microswimmers is more complex. Our findings suggest that, by selecting the size of the obstacles, we can control the accumulation near the surface. Covering a surface with obstacles could make it more resistant to the accumulation of microswimmers that are only weakly chiral (that swim in orbits larger than the size of the obstacles), but less resistant to strongly chiral swimmers (that swim in orbits with the size of the obstacles or smaller).

Additionally, the surface accumulation of swimmers of different chiralities, or the tendency of swimmers to accumulate at obstacles that are larger than the radius of their swimming orbit, could be used to design a sorter of microswimmers based on their angular velocity. By selecting from a mixture of microswimmers the most appropriate swimming

properties, the efficiency of microswimmers for a specific task, e.g., drug-delivery or bioremediation, might be improved [42,49]. Alternatively, chirality-based spermatozoa selection may be employed to select cells with specific swimming traits desirable for artificial fertilization techniques [50,52]. Our results suggest that, for chiral swimmers with a rotational diffusion similar to that of bull sperm, effective sorting by angular velocity could be achieved. Future work might include differently shaped obstacles that are known to trap swimmers well to further explore this idea.

In recent studies, for a microswimmer following a convex boundary, the angle between swimmer and boundary was found to depend on the radius of curvature of the boundary [11,12]. By making the alignment force dependent on the radius of curvature we could explicitly include this in our model. An interesting extension of this work would be to investigate the effect of varying the distance between the surfaces or thickness of the channel. Preliminary results indicate that when the thickness is varied this especially affects the accumulation of swimmers that do not get trapped on the surface but instead attach/detach intermittently. As the distance is increased, these swimmers tend to spend more time in the volume between the surfaces, reducing surface accumulation. For parameters that result in trapping, this effect is not observed. Alternatively, in [44] the swimming behavior of an active particle between obstacles, resulting in optimal space exploration, was found to be different for convex and concave obstacles. In the future, the effect of cavities (or concave obstacles) on surface accumulation of microswimmers could also be explored in combination with convex obstacles. In [44] the active particles were confined to a surface, while with the model proposed here, it would be possible to extend this study to 3D domains.

ACKNOWLEDGMENTS

We acknowledge financial support by the European Commissions Horizon 2020 research and innovation program under the Marie Sklodowska-Curie Grant Agreement No. 812780 and from the Portuguese Foundation for Science and Technology (FCT) under Contracts No. UIDB/00618/2020 and No. UIDP/00618/2020. N.A.M.A. and G.V. also acknowledge support from the UCL MAPS Faculty Visiting Fellowship programme.

^[1] G. Gompper, R. G. Winkler, T. Speck, A. Solon, C. Nardini, F. Peruani, H. Löwen, R. Golestanian, U. B. Kaupp, L. Alvarez, T. Kiørboe, E. Lauga, W. C. K. Poon, A. DeSimone, S. Muiños-Landin, A. Fischer, N. A. Söker, F. Cichos, R. Kapral, P. Gaspard, M. Ripoll, F. Sagues, A. Doostmohammadi, J. M. Yeomans, I. S. Aranson, C. Bechinger, H. Stark, C. K. Hemelrijk, F. J. Nedelec, T. Sarkar, T. Aryaksama, M. Lacroix, G. Duclos, V. Yashunsky, P. Silberzan, M. Arroyo, and S. Kale, J. Phys.: Condens. Matter 32, 193001 (2020).

^[2] G. Volpe, C. Bechinger, F. Cichos, R. Golestanian, H. Löwen, M. Sperl, and G. Volpe, npj Microgravity 8, 54 (2022).

^[3] C. Bechinger, R. Di Leonardo, H. Löwen, C. Reichhardt, G. Volpe, and G. Volpe, Rev. Mod. Phys. 88, 045006 (2016).

^[4] J. Elgeti, R. G. Winkler, and G. Gompper, Rep. Prog. Phys. 78, 056601 (2015).

^[5] S. Makarchuk, V. Braz, N. Araujo, L. Ciric, and G. Volpe, Nat. Commun. 10, 4110 (2019).

^[6] K. Yang, J. Shi, L. Wang, Y. Chen, C. Liang, L. Yang, and L.-N. Wang, J. Mater. Sci. Technol. 99, 82 (2022).

^[7] N. A. M. Araújo, L. M. C. Janssen, T. Barois, G. Boffetta, I. Cohen, A. Corbetta, O. Dauchot, M. Dijkstra, W. M. Durham, A. Dussutour, S. Garnier, H. Gelderblom, R. Golestanian, L. Isa, G. H. Koenderink, H. Löwen, R. Metzler, M. Polin, C. P.

- Royall, A. Šarić, A. Sengupta, C. Sykes, V. Trianni, I. Tuval, N. Vogel, J. M. Yeomans, I. Zuriguel, A. Marin, and G. Volpe, Soft Matter 19, 1695 (2023).
- [8] J. Elgeti and G. Gompper, Eur. Phys. J.: Spec. Top. 225, 2333 (2016).
- [9] A. P. Berke, L. Turner, H. C. Berg, and E. Lauga, Phys. Rev. Lett. 101, 038102 (2008).
- [10] D. Takagi, J. Palacci, A. Braunschweig, M. Shelley, and J. Zhang, Soft Matter 10, 1784 (2014).
- [11] S. E. Spagnolie, G. R. Moreno-Flores, D. Bartolo, and E. Lauga, Soft Matter 11, 3396 (2015).
- [12] O. Sipos, K. Nagy, R. Di Leonardo, and P. Galajda, Phys. Rev. Lett. 114, 258104 (2015).
- [13] E. Lauga, W. R. DiLuzio, G. M. Whitesides, and H. A. Stone, Biophys. J. 90, 400 (2006).
- [14] B. Liebchen and D. Levis, Europhys. Lett. 139, 67001 (2022).
- [15] J. Elgeti, U. Kaupp, and G. Gompper, Biophys. J. 99, 1018 (2010).
- [16] E. Perez Ipiña, S. Otte, R. Pontier-Bres, D. Czerucka, and F. Peruani, Nat. Phys. 15, 610 (2019).
- [17] M. P. Schultz, J. A. Bendick, E. R. Holm, and W. M. Hertel, Biofouling **27**, 87 (2011).
- [18] G. D. Bixler and B. Bhushan, Phil. Trans. R. Soc. 370, 2381 (2012).
- [19] J. Fiedler, A. Kolitsch, B. Kleffner, D. Henke, S. Stenger, and R. E. Brenner, Int. J. Artif. Organs 34, 882 (2011).
- [20] G.-D. Kang and Y. ming Cao, Water Res. 46, 584 (2012).
- [21] Z. Khatoon, C. D. McTiernan, E. J. Suuronen, T.-F. Mah, and E. I. Alarcon, Heliyon 4, e01067 (2018).
- [22] P. S. Leonov, X. Flores-Alsina, K. V. Gernaey, and C. Sternberg, Biotechnol. Adv. 50, 107766 (2021).
- [23] J. Gadkari, S. Bhattacharya, and A. Shrivastav, *Development in Wastewater Treatment Research and Processes* (Elsevier, Amsterdam, 2022), Chap. 7, pp. 153–173.
- [24] M. Dade-Robertson, A. Keren-Paz, M. Zhang, and I. Kolodkin-Gal, Microb. Biotechnol. 10, 1157 (2017).
- [25] Y. Luan, S. Liu, M. Pihl, H. van der Mei, J. Liu, F. Hizal, C.-H. Choi, H. Chen, Y. Ren, and H. Busscher, Curr. Opin. Colloid Interface Sci. 38, 170 (2018).
- [26] J. Shi, S. Wang, X. Cheng, S. Chen, and G. Liu, J. Mater. Sci. Technol. 70, 145 (2021).
- [27] S. B. Chinnaraj, P. G. Jayathilake, J. Dawson, Y. Ammar, J. Portoles, N. Jakubovics, and J. Chen, J. Mater. Sci. Technol. 81, 151 (2021).

- [28] J. Hu, A. Wysocki, R. G. Winkler, and G. Gompper, Sci. Rep. 5, 9586 (2015).
- [29] A. Dehkharghani, N. Waisbord, and J. S. Guasto, Commun. Phys. 6, 18 (2023).
- [30] M. Zeitz, K. Wolff, and H. Stark, Eur. Phys. J. E 40, 23 (2017).
- [31] O. Chepizhko and T. Franosch, Soft Matter 15, 452 (2019).
- [32] O. Chepizhko and T. Franosch, New J. Phys. 22, 073022 (2020).
- [33] D. M. van Roon, G. Volpe, M. M. Telo da Gama, and N. A. M. Araújo, Soft Matter 18, 6899 (2022).
- [34] A. T. Brown, I. D. Vladescu, A. Dawson, T. Vissers, J. Schwarz-Linek, J. S. Lintuvuori, and W. C. K. Poon, Soft Matter 12, 131 (2016).
- [35] A. Weber, M. Bahrs, Z. Alirezaeizanjani, X. Zhang, C. Beta, and V. Zaburdaev, Front. Phys. 7, 148 (2019).
- [36] M. Brun-Cosme-Bruny, E. Bertin, B. Coasne, P. Peyla, and S. Rafaï, J. Chem. Phys. 150, 104901 (2019).
- [37] C. Kurzthaler, S. Mandal, T. Bhattacharjee, H. Löwen, S. Dattaf, and H. Stone, Nat. Commun. 12, 7088 (2021).
- [38] S. Bianchi, F. Saglimbeni, and R. Di Leonardo, Phys. Rev. X 7, 011010 (2017).
- [39] S. Bianchi, F. Saglimbeni, G. Frangipane, D. Dell'Arciprete, and R. Di Leonardo, Soft Matter 15, 3397 (2019).
- [40] K. Drescher, J. Dunkel, L. H. Cisneros, S. Ganguly, and R. E. Goldstein, Proc. Natl. Acad. Sci. 108, 10940 (2011).
- [41] G. Li and J. X. Tang, Phys. Rev. Lett. 103, 078101 (2009).
- [42] M. Mijalkov and G. Volpe, Soft Matter 9, 6376 (2013).
- [43] G. Volpe, S. Gigan, and G. Volpe, Am. J. Phys. 82, 659 (2014).
- [44] G. Volpe and G. Volpe, Proc. Natl. Acad. Sci. USA 114, 11350 (2017).
- [45] K. J. Modica, Y. Xi, and S. C. Takatori, Front. Phys. 10, 869175 (2022).
- [46] M. R. Shaebani, A. Wysocki, R. G. Winkler, G. Gompper, and H. Rieger, Nat. Rev. Phys. 2, 181 (2020).
- [47] M. R. Bailey, C. M. Barriuso Gutiérrez, J. Martín-Roca, V. Niggel, V. Carrasco-Fadanelli, I. Buttinoni, I. Pagonabarraga, L. Isa, and C. Valeriani, Nanoscale 16, 2444 (2024).
- [48] T. Laird, Org. Process Res. Dev. 15, 946 (2011).
- [49] L. Fu and C. L. Kane, Phys. Rev. Lett. 102, 216403 (2009).
- [50] B. Nath, L. Caprini, C. Maggi, A. Zizzari, V. Arima, I. Viola, R. Di Leonardo, and A. Puglisi, Lab Chip 23, 773 (2023).
- [51] S. van Teeffelen and H. Löwen, Phys. Rev. E 78, 020101 (2008).
- [52] I. Oseguera-López, S. Ruiz-Díaz, P. Ramos-Ibeas, and S. Pérez-Cerezales, Front. Cell Dev. Biol. **7**, 23 (2019).